HHS Public Access

Author manuscript

Radiology. Author manuscript; available in PMC 2016 October 01.

Published in final edited form as:

Radiology. 2016 October ; 281(1): 193–202. doi:10.1148/radiol.2016151155.

Comparison of Whole-Body ^{18}F FDG PET/MR Imaging and Whole-Body ^{18}F FDG PET/CT in Terms of Lesion Detection and Radiation Dose in Patients with Breast Cancer

Amy N. Melsaether, MD, **Roy A. Raad, MD**, **Akshat C. Pujara, MD**, **Fabio D. Ponzo, MD**, **Kristine M. Pysarenko, MD**, **Komal Jhaveri, MD**[2], **James S. Babb, PhD**, **Eric E. Sigmund, PhD**, **Sungheon G. Kim, PhD**, and **Linda A. Moy, MD**

Department of Radiology, NYU Perlmutter Cancer Center, New York University School of Medicine, 160 E 34th St, 3rd Floor, New York, NY 10014

Abstract

Purpose—To compare fluorine 18 (^{18}F) fluorodeoxyglucose (FDG) combined positron emission tomography (PET) and magnetic resonance (MR) imaging with ^{18}F FDG combined PET and computed tomography (CT) in terms of organ-specific metastatic lesion detection and radiation dose in patients with breast cancer.

Materials and Methods—From July 2012 to October 2013, this institutional review board–approved HIPAA-compliant prospective study included 51 patients with breast cancer (50 women; mean age, 56 years; range, 32–76 years; one man; aged 70 years) who completed PET/MR imaging with diffusion-weighted and contrast material–enhanced sequences after unenhanced PET/CT. Written informed consent for study participation was obtained. Two independent readers for each modality recorded site and number of lesions. Imaging and clinical follow-up, with consensus in two cases, served as the reference standard.

Results—There were 242 distant metastatic lesions in 30 patients, 18 breast cancers in 17 patients, and 19 positive axillary nodes in eight patients. On a per-patient basis, PET/MR imaging with diffusion-weighted and contrast-enhanced sequences depicted distant (30 of 30 [100%] for readers 1 and 2) and axillary (eight of eight [100%] for reader 1, seven of eight [88%] for reader 2) metastatic disease at rates similar to those of unenhanced PET/CT (distant metastatic disease: 28 of 29 [96%] for readers 3 and 4, $P = .50$; axillary metastatic disease: seven of eight [88%] for

Address correspondence to A.N.M. (amy.melsaether@nyumc.org).

[2]**Current address:**

Breast Medicine Service, Department of Medicine, Memorial Sloan Kettering Cancer Center/Evelyn H. Lauder Breast and Imaging Center, New York, NY.

Online supplemental material is available for this article.

Author contributions: Guarantors of integrity of entire study, A.N.M., R.A.R., K.M.P., L.A.M.; study concepts/study design or data acquisition or data analysis/interpretation, all authors; manuscript drafting or manuscript revision for important intellectual content, all authors; approval of final version of submitted manuscript, all authors; agrees to ensure any questions related to the work are appropriately resolved, all authors; literature research, A.N.M., A.C.P., K.M.P., L.A.M.; clinical studies, A.N.M., R.A.R., A.C.P., F.D.P., K.M.P., S.G.K., L.A.M.; statistical analysis, J.S.B.; and manuscript editing, all authors

Disclosures of Conflicts of Interest: A.N.M. disclosed no relevant relationships. **R.A.R.** disclosed no relevant relationships. **A.C.P.** disclosed no relevant relationships. **F.D.P.** disclosed no relevant relationships. **K.M.P.** disclosed no relevant relationships. **K.J.** disclosed no relevant relationships. **J.S.B.** disclosed no relevant relationships. **E.E.S.** disclosed no relevant relationships. **S.G.K.** disclosed no relevant relationships. **L.A.M.** disclosed no relevant relationships.

readers 3 and 4, $P > .99$) and outperformed PET/CT in the detection of breast cancer (17 of 17 [100%] for readers 1 and 2 vs 11 of 17 [65%] for reader 3 and 10 of 17 [59%] for reader 4; $P < .001$). PET/MR imaging showed increased sensitivity for liver (40 of 40 [100%] for reader 1 and 32 of 40 [80%] for reader 2 vs 30 of 40 [75%] for reader 3 and 28 of 40 [70%] for reader 4; $P < .001$) and bone (105 of 107 [98%] for reader 1 and 102 of 107 [95%] for reader 2 vs 106 of 107 [99%] for reader 3 and 93 of 107 [87%] for reader 4; $P = .012$) metastases and revealed brain metastases in five of 51 (10%) patients. PET/CT trended toward increased sensitivity for lung metastases (20 of 23 [87%] for reader 1 and 17 of 23 [74%] for reader 2 vs 23 of 23 [100%] for reader 3 and 22 of 23 [96%] for reader 4; $P = .065$). Dose reduction averaged 50% ($P < .001$).

Conclusion—In patients with breast cancer, PET/MR imaging may yield better sensitivity for liver and possibly bone metastases but not for pulmonary metastases, as compared with that attained with PET/CT, at about half the radiation dose.

Whole-body fluorine 18 (^{18}F) fluorodeoxyglucose (FDG) combined positron emission tomography (PET) and computed tomography (CT) is commonly performed in patients suspected of having recurrent or metastatic breast cancer and to evaluate response to therapy (1,2). Recently, PET/CT has been shown to depict distant metastatic disease in 20% of patients with newly diagnosed stage IIb or stage III breast cancer, suggesting a wider role in initial staging (3).

However, PET/CT entails a relatively high radiation dose (4,5), and low sensitivities for brain (6,7) and liver (8) lesions have been reported. These sites are particularly important in the early detection of metastases, as local treatment of liver (9,10) and brain (11,12) lesions has been shown to improve survival, local control, and quality of life.

Several initial studies have compared whole-body combined PET and magnetic resonance (MR) imaging with PET/CT and have shown similar performance for bone (13–16) and lymph node (15,17,18) metastases in mixed adult and pediatric (19) oncologic populations. Performance for liver metastases has been mixed, with one study reporting fewer metastases seen on PET/MR images (15) and another study reporting equivalent detection but superior conspicuity with PET/MR imaging (20). Specifically, in patients with breast cancer, one study in 36 patients focused on FDG-avid lesions and showed equivalent performance between PET/MR imaging and PET/CT in the anatomic allocation of lymph node, bone, and lung metastases (21), but the study did not include liver metastases. A second study in 36 patients addressed PET/MR imaging in patients with breast cancer; however, this study compared performance with PET alone rather than performance with PET/CT (22).

We hypothesized that in patients with breast cancer, diffusion-weighted and contrast material–enhanced PET/MR imaging sequences would yield increased metastatic lesion sensitivity, apart from pulmonary metastases, at a decreased radiation dose, as compared with PET/CT.

The purpose of this study was to compare PET/MR imaging with PET/CT in terms of organ-specific metastatic lesion detection and radiation dose in patients with breast cancer.

Materials and Methods

This prospective study was approved by our institutional review board and was compliant with the Health Insurance Portability and Accountability Act. Written informed consent for study participation was obtained. Between July 2012 and October 2013, 351 consecutive patients with a breast cancer diagnosis who were scheduled for clinical PET/CT were contacted by the research coordinator. Fifty-four patients without one or more contraindications to MR imaging and with no additional cancer diagnoses consented to undergo whole-body PET/MR imaging immediately after PET/CT. Three patients did not complete PET/MR imaging due to discomfort and were excluded. In total, 51 patients (50 women; age range, 32–76 years; mean age, 56 years; one man aged 70 years) were included. Ten subjects were also included in a pulmonary nodule study (23), and 33 subjects were included in a study comparing CT- and MR-based attenuation correction (24).

Indications for PET/CT included response to chemotherapy ($n = 26$), surveillance in patients with quiescent metastatic disease ($n = 13$), initial staging at the time of diagnosis ($n = 6$), suspected recurrence ($n = 3$), known recurrence in the breast ($n = 2$), and abnormal chest CT findings ($n = 1$). Patient demographics, pathology results, additional imaging studies, and clinical information were culled from the electronic medical record.

^{18}F FDG PET/CT

Prior to ^{18}F FDG PET/CT, patients fasted for at least 4 hours. When applicable, insulin was withheld for 6 hours. Blood glucose level was verified to be lower than 200 mg/dL (11.1 mmol/L). Intravenous ^{18}F FDG (mean dose, 547.6 MBq; range, 484.7–566.1 MBq) was administered. Patients then rested for 45 minutes and were asked to void before imaging. PET/CT was performed from the vertex to the thighs ($n = 24$) or, due to an error in protocol, from the skull base to the thighs ($n = 27$) by using a Biograph mCT imager (Siemens Healthcare, Knoxville, Tenn). All patients received oral barium contrast material. Intravenous contrast material was not administered. The PET/CT unit has a lutetium oxyorthosilicate crystal and a photomultiplier tube. Acquisition parameters for CT include peak voltage of 120 kVp (Care Dose4D; Siemens Healthcare, Erlangen, Germany), modulation with a reference tube current of 95 mA, rotation time of 0.3–0.5 second, and collimation of 16.0 × 1.2 mm. PET data were acquired with an imaging time of 2–3 minutes per bed position for a total examination time of less than 25 minutes and were reconstructed by using standard software provided by the vendor with a three-dimensional ordinary Poisson ordered-subset expectation maximization algorithm, two iterations, 21 subsets, and a 2-mm Gaussian filter (image matrix, 168 × 168; voxel size, 1.78 × 1.78 × 2.00 mm).

PET/MR Imaging

PET and MR imaging data were acquired simultaneously by using the 3-T Biograph MR system (Siemens Healthcare, Knoxville, Tenn) a mean of 167 minutes ± 36 (standard deviation) (range, 131–203 minutes) after ^{18}F FDG injection for PET/CT. Examination from the thighs to the vertex was conducted with the patient in the supine position by using a dedicated multichannel head and neck coil and a set of flexible body matrix coils. The examination consisted of *(a)* a three-dimensional volumetric interpolated breath-hold

examination Dixon sequence performed for MR attenuation correction (Dixon-based four-segment μ map), *(b)* a T1-weighted radial stack-of-stars three-dimensional spoiled gradient-echo sequence (radial volumetric interpolated breath-hold examination) with golden-angle spoke ordering and frequency-selected fat suppression, and *(c)* a two-dimensional double-refocused echo-planar diffusion-weighted imaging sequence with spectral attenuated inversion fat suppression and three diffusion directions. Sequence parameters are detailed in Table E1 (online). Rapid intravenous bolus injection of 0.1 mmol/L gadopentetate dimeglumine (Magnevist; Bayer, Leverkusen, Germany) per kilogram of body weight was administered at a rate of 2.0 mL/sec during the liver station. PET events were accumulated for 6 minutes per station for a total examination time of less than 45 minutes. Images were reconstructed by using the vendor platform.

Image Interpretation

All PET/CT and PET/MR images were interpreted by two independent readers using XD3 software (version 3.6; Mirada Medical, Oxford, England) who were blinded to patient history. PET/MR image readers were two radiologists, one with 2 years of PET/MR experience (reader 1, A.N.M.) and one with brief training in PET/MR image interpretation (ie, five co-read studies prior to this study) (reader 2, K.M.P.). PET/CT image readers were one nuclear medicine physician (reader 3, F.D.P.) and one radiologist (reader 4, R.A.R.) with 13 years and 1 year of PET/CT experience, respectively. Site and number of lesions seen with each imaging sequence were recorded. Lesions the reader interpreted as *(a)* definite metastases or *(b)* indeterminate, requiring additional testing, were considered positive findings. Up to six lesions per organ per patient were included to limit bias from any one organ in any one patient.

Whole-body follow-up examinations were performed in 40 patients (mean follow-up, 19 months; range, 5–30 months). Abdominal MR images were available in six patients, and axillary node and breast pathology results were available in eight and 17 patients, respectively. Bone and distant node biopsy results were available in one patient and three patients, respectively. In three patients with otherwise equivocal lung nodules, PET/CT images obtained more than 36 months prior to the current examination were used for comparison, with stability recorded as benignity. Of 11 patients who did not undergo whole-body imaging follow-up, nine had no evidence of metastatic disease and were followed clinically without evidence of recurrence (mean, 20 months; range, 7–28 months). One patient with no evidence of disease and one patient with metastatic disease had no follow-up data (one patient transferred care, one patient died). In these two patients, consensus served as the reference standard; there were no disagreements.

Radiation Dose

Effective dose (ED) due to the PET portion of the examination (ED^{PET}) was calculated as follows:

$$ED^{PET} = AD^{FDG} \times 0.017.$$

AD^{FDG} is the administered dose, and 0.017mSv/MBq is the whole-body ED coefficient recommended by Brix et al (25) based on International Commission on Radiation Protection publication 103 (26).

ED due to the CT portion of the examination (ED^{CT}) was estimated according to the method described by Huda et al (27), in which the vendor-provided CT dose-length product (DLP) is converted to ED via the ED-to-DLP ratio. The ED-to-DLP ratio for whole-body scans is reported as 15.4 uSv/mGy at 120 kV (28), based on International Commission on Radiological Protection publication 103 tissue-weighting factors (26). The equation used to calculate ED^{CT} is as follows:

$$ED^{CT} = DLP \times 15.4/1000.$$

Statistical Analysis

Logistic regression for correlated data was used to assess and compare imaging modalities (PET/MR imaging and PET/CT) in terms of diagnostic accuracy in the detection of systemic metastases, breast cancer, axillary nodal disease, and lesions within each organ system. Specifically, generalized estimating equations based on binary logistic regression analysis were used to model the binary indicator of agreement between the reference standard and reader-based diagnoses as a function of imaging modality while accounting for the lack of statistical independence among results derived from the same patient. Statistical tests were conducted at the two-sided 5% significance level by using statistical software (SAS, version 9.3; SAS Institute, Cary, NC). *P* values and 95% confidence intervals for sensitivity and specificity of each modality were derived from these generalized estimating equations, in which the individual results from the two readers were combined in one vector that served as the dependent variable for analysis.

One patient had brain metastases that were imaged only at PET/MR imaging because PET/CT did not extend to the vertex. Thus, this patient was included as having metastatic disease in PET/MR imaging results but was excluded as having metastatic disease in PET/CT results.

Interreader agreement between PET/MR imaging readers and between PET/CT readers was assessed in terms of the simple κ coefficient, a 95% confidence interval for κ, and the percentage of times the readers evaluating images obtained with the same modality provided a concordant assessment in terms of the presence or absence of at least one lesion in the indicated organ system. A κ value of less than zero generally indicates poor agreement, a κ value of 0–0.20, slight agreement; a κ value of 0.21–0.40, fair agreement; a κ value of 0.41–0.60, moderate agreement; and a κ value of 0.60 or more, substantial agreement.

The paired Student *t* test was used to compare PET/CT and PET/MR imaging radiation doses. A 95% confidence interval for the difference between PET/MR imaging and PET/CT was assessed in terms of radiation dose.

Results

There were 242 distant metastatic lesions in 30 patients (Table 1), 18 breast cancers in 17 patients, and 19 axillary nodes with positive findings in eight patients. Thirteen patients had no primary (previously excised) or metastatic disease. PET/CT and PET/MR imaging showed similar subject-level performance for distant and axillary metastatic disease. PET/MR imaging was more sensitive for breast cancers ($P < .001$) (Table 1).

In the liver, PET/MR imaging depicted increased lesion-level sensitivity versus PET/CT (100% for reader 1 and 80% for reader 2 vs 75% for reader 3 and 70% for reader 4, $P < .001$) (Table 2), but this increased sensitivity was not significant at the patient level (100% for reader 1 and 91% for reader 2 vs 73% for both reader 3 and reader 4, $P = .095$) (Table E2 [online], Table 3). Metastases were seen on only PET/MR images in three patients, one of whom was classified as free of disease with PET/CT; reader 1 noted one false-positive lesion (hemangioma), which prompted liver MR imaging. Increased detection of metastases was due to diffusion-weighted imaging, which depicted up to 40 metastases, whereas PET depicted up to 28 metastases and contrast-enhanced T1-weighted imaging depicted up to 27 metastases (Table 4, Fig 1).

In the lung, subject-level pulmonary metastatic disease detection was similar between PET/MR imaging and PET/CT (100% for reader 1 and 83% for reader 2 vs 100% for both reader 3 and reader 4, $P > .99$) (Table E2 [online], Table 3); however, PET/CT trended toward increased lesion-level sensitivity (100% for reader 3 and 96% for reader 4 vs 87% for reader 1 and 74% for reader 2, $P = .065$) (Fig 2, Table 2). PET/MR imaging had greater subject-level specificity (89% for reader 1 and 99% for reader 2 vs 80% for reader 3 and 82% for reader 4, $P = .008$) (Table E2 [online], Table 3). False-positive results were due to *(a)* infection (two or three patients per reader), *(b)* subcentimeter nodules that resolved at follow-up imaging in the face of otherwise progressive disease (two to four patients per reader), and *(c)* subcentimeter nodules that were not FDG avid, were seen on only PET/CT images, and were stable over at least 36 months of prior examinations (two or three lesions per PET/CT reader). False-positive lung findings were the only sign of metastatic disease in four patients; in two of these patients, false-positive results occurred in only the CT portion of the PET/CT examination.

In bone, subject-level detection of osseous metastatic disease was similar between modalities (100% for both reader 1 and reader 2 vs 96% for both reader 3 and reader 4, $P > .99$) (Table E2 [online], Table 3), but PET/MR imaging demonstrated increased lesion-level sensitivity (98% for reader 1 and 95% for reader 2 vs 99% for reader 3 and 87% for reader 4, $P = .012$) (Table 2). PET/CT readers did not see osseous metastatic disease in one patient each; however, this was not the same patient.

In this study, five (10%) of 51 patients had brain metastases. Reader 1 detected 15 (100%) of 15 metastases in five (100%) of five patients, and reader 2 detected 14 (93%) of 15 metastases in four (80%) of five patients. As noted in Materials and Methods, the brain was included in 24 of 51 PET/CT examinations, and only one of these patients had brain metastases. No brain metastases were seen on PET/CT images. In one patient undergoing

initial staging, brain metastases were the only evidence of metastatic disease. In one patient, brain metastases were seen in the setting of other metastatic disease, and in one patient, a lesion previously treated with gamma knife therapy was shown to have recurred. In two patients, brain metastases were known from prior imaging. All 15 brain metastases were seen on contrast-enhanced T1-weighted images, and seven were seen on diffusion-weighted images (Table 4, Fig E1 [online]).

Interreader Agreement

Interreader agreement in terms of the presence or absence of at least one lesion in the indicated organ system was substantial for all organs for both PET/MR imaging and PET/CT readers (Table E3 [online]). Overall, the more experienced readers (readers 1 and 3) detected more metastatic lesions than did the less experienced readers (readers 2 and 4).

Radiation Dose

CT ED ranged from 2.2 to 16.9 mSv (mean, 8.3 mSv). PET ED (equivalent to PET/MR imaging ED) ranged from 8.2 to 9.9 mSv (mean, 9.3 mSv). PET/CT ED ranged from 11.7 to 26.3 mSv (mean, 17.6 mSv). Dose reduction if PET/MR imaging had been performed instead of PET/CT ranged from 18.9% to 64.3% (mean, 50.0%) ($P < .001$). The 95% confidence interval for the mean reduction in dose extended from 7.40 to 9.16 mSv.

Discussion

Previously published works on PET/MR imaging in patients with breast cancer include *(a)* a study by Pace et al (21) that included 14 distant metastases (three lung and 11 skeletal lesions) and showed PET/MR imaging performs as well as PET/CT in the anatomic allocation of PET-positive lesions and *(b)* a study by Taneja et al (22) that showed that in eight patients with metastatic disease, PET/MR imaging depicted more systemic metastases than did PET alone. In comparing lesion detection on PET/MR images with lesion detection on PET/CT images, rather than focusing on the appearance of PET-positive lesions with each modality (21) or on lesion detection between PET/MR imaging and PET alone (22), our current study was more focused on whether PET/MR imaging could be substituted for PET/CT in the evaluation of patients with breast cancer in clinical practice.

In our study, PET/CT did not depict hepatic disease seen at PET/MR imaging in three of 11 patients; however, this difference was not significant ($P = .095$), perhaps because of the sample size. On a per-lesion level, PET/MR imaging did outperform PET/CT ($P < .001$). Kuhn et al (20) also suggest PET/MR imaging may be preferable, reporting equivalent hepatic lesion detection ($n = 51$) but greater conspicuity at PET/MR imaging. Studies including up to 11 lesions show equivalent or nearly equivalent results (15,16,19).

For pulmonary nodule assessment, several authors report that detection of FDG-avid nodules with PET/MR imaging is similar to that with PET/CT (15,18,21,23,29,30) and that PET/MR imaging is less sensitive for nodules that are not FDG avid and for small pulmonary nodules (23,29). Although we saw no difference in subject-level detection of pulmonary metastatic disease, PET/MR imaging did depict fewer pulmonary metastases overall ($P = .065$), and caution is still recommended in PET/MR imaging evaluation of pulmonary metastases.

Catalano et al (31) showed that PET/MR imaging depicted osseous metastases in significantly more patients with breast cancer ($n = 25$) as compared with PET/CT, while several smaller mixed-population studies have shown similar detection rates (13–16,19,21). We show similar subject-level detection with increased lesion-level sensitivity ($P = .012$) in concordance with other reports that PET/MR imaging yields increased conspicuity for osseous lesions (14,20). However, our results show decreased sensitivity for reader 4 (87%), as compared with that for the other readers (range, 95%–99%).

Brain metastases are common among patients with breast cancer, they are treatable (12), and they were seen on PET/MR images in 10% of these patients. Although PET/CT did not include the brain in over half of these patients, available data suggest PET/CT depicts only 50%–70% of known presumably symptomatic brain metastases (6,7). Accordingly, the 15 brain metastases in our study were seen on contrast-enhanced MR images and not on simultaneously acquired PET images.

In this study, PET/MR imaging depicted breast cancers in significantly more patients than did PET/CT ($P < .001$), whereas Pace et al (21) report similar performance for the two modalities. This difference is because MR imaging is more sensitive than PET in the detection of breast cancers (Table 4) (22,32,33), and Pace et al (21) included only PET-positive lesions, which were then localized on MR and CT images. Nevertheless, supine whole-body imaging cannot substitute for properly positioned dedicated breast imaging.

Finally, radiation doses that are as low as reasonably achievable are particularly salient in breast cancer imaging, as 7% of patients receive a breast cancer diagnosis before 40 years of age and one in 30 women receive a breast cancer diagnosis by 55 years of age (34). With 5-year survival rates approximating 85% (35), there are concerns for subsequent radiation-induced cancers. Intuitively, the radiation dose due to PET/MR imaging will be lower than that due to PET/CT, and here we calculate an average dose reduction of 8.3 mSv (50%). The CT protocols performed with PET vary between institutions, so dose savings reported here may be higher or lower than those reported elsewhere.

There were several limitations in this study. Similar to previous studies (12–19,21,23), our FDG uptake times were longer for PET/MR imaging than for PET/CT, which could allow for greater lesion conspicuity at the delayed examination. However, we found the diffusion-weighted sequence accounted for the detection of additional liver metastases and the contrast-enhanced T1-weighted sequence accounted for the detection of brain metastases. Our PET/MR imaging protocol included contrast material, while our PET/CT protocol did not. CT contrast material is not routinely used in our clinical PET/CT protocol. Gadolinium-containing contrast agents have a preferable safety profile and would likely be used with clinical PET/MR imaging. The patient cohort in this study was a heterogeneous population at an academic center imaged at various points in their disease. In this population, treated inactive metastases, especially those in bone and liver, could be confounding. However, positivity for FDG-negative lesions was determined by progression at follow-up examinations. Stable FDG-negative lesions, such as treated metastases, were not included as positive lesions. Disease at an academic center may be more severe than that in the community. The four readers in this study may have had variable diagnostic abilities, which

may have led to differences that we attributed to the modality. Imaging follow-up, particularly abdominal MR imaging, may be biased toward patients with findings on PET/MR images. Finally, pathology data are not available for almost all lesions and, as such, imaging and clinical follow-up with rare consensus served as the reference standard.

In regard to radiation dose calculation, ED-to-DLP ratio conversion factors are based on a constant 120-keV x-ray tube output, while our CT protocol includes a modulated current. Studies on the effect of tube current modulation on dose have suggested ED-to-DLP ratio conversion factors would be reduced, though not by a large amount (2%–9%) (36).

In summary, in patients with breast cancer, whole-body PET/MR imaging with diffusion-weighted and contrast-enhanced sequences depicts metastatic disease at a rate similar to that of PET/CT; is more sensitive for breast cancers, liver metastases, and possibly bone metastases but not pulmonary metastases; depicts brain metastases; and requires approximately half the radiation dose of PET/CT.

These data may suggest particular roles for PET/MR imaging at initial staging *(a)* in young women, *(b)* when the detection of hepatic metastases allows for local treatment (9,10), *(c)* in response to rising tumor markers when PET/MR imaging may better depict a recurrent cancer in the breast, *(d)* in patients undergoing serial imaging, and *(e)* in patients with *HER2*-positive and basal-like breast cancers, upwards of 30% of whom may have brain metastases (37).

Abbreviations

DLP	dose-length product
ED	effective dose
FDG	fluorodeoxyglucose

References

1. Kamel EM, Wyss MT, Fehr MK, von Schulthess GK, Goerres GW. [18F]-Fluorodeoxyglucose positron emission tomography in patients with suspected recurrence of breast cancer. J Cancer Res Clin Oncol. 2003; 129(3):147–153. [PubMed: 12712329]
2. Moon DH, Maddahi J, Silverman DH, Glaspy JA, Phelps ME, Hoh CK. Accuracy of whole-body fluorine-18-FDG PET for the detection of recurrent or metastatic breast carcinoma. J Nucl Med. 1998; 39(3):431–435. [PubMed: 9529287]
3. Groheux D, Hindié E, Delord M, et al. Prognostic impact of (18)FDG-PET-CT findings in clinical stage III and IIB breast cancer. J Natl Cancer Inst. 2012; 104(24):1879–1887. [PubMed: 23243198]
4. Huang B, Law MW, Khong PL. Whole-body PET/CT scanning: estimation of radiation dose and cancer risk. Radiology. 2009; 251(1):166–174. [PubMed: 19251940]
5. Brix G, Lechel U, Glatting G, et al. Radiation exposure of patients undergoing whole-body dual-modality 18F-FDG PET/CT examinations. J Nucl Med. 2005; 46(4):608–613. [PubMed: 15809483]
6. Griffeth LK, Rich KM, Dehdashti F, et al. Brain metastases from non-central nervous system tumors: evaluation with PET. Radiology. 1993; 186(1):37–44. [PubMed: 8416584]
7. Kitajima K, Nakamoto Y, Okizuka H, et al. Accuracy of whole-body FDG-PET/CT for detecting brain metastases from non-central nervous system tumors. Ann Nucl Med. 2008; 22(7):595–602. [PubMed: 18756362]

8. Rappeport ED, Loft A, Berthelsen AK, et al. Contrast-enhanced FDG-PET/CT vs. SPIO-enhanced MRI vs. FDG-PET vs. CT in patients with liver metastases from colorectal cancer: a prospective study with intraoperative confirmation. Acta Radiol. 2007; 48(4):369–378. [PubMed: 17453514]
9. Selzner M, Morse MA, Vredenburgh JJ, Meyers WC, Clavien PA. Liver metastases from breast cancer: long-term survival after curative resection. Surgery. 2000; 127(4):383–389. [PubMed: 10776428]
10. Mack MG, Straub R, Eichler K, Söllner O, Lehnert T, Vogl TJ. Breast cancer metastases in liver: laser-induced interstitial thermotherapy—local tumor control rate and survival data. Radiology. 2004; 233(2):400–409. [PubMed: 15459328]
11. Patchell RA, Tibbs PA, Walsh JW, et al. A randomized trial of surgery in the treatment of single metastases to the brain. N Engl J Med. 1990; 322(8):494–500. [PubMed: 2405271]
12. De Ieso PB, Schick U, Rosenfelder N, Mohammed K, Ross GM. Breast cancer brain metastases: a 12 year review of treatment outcomes. Breast. 2015; 24(4):426–433. [PubMed: 25881974]
13. Eiber M, Takei T, Souvatzoglou M, et al. Performance of whole-body integrated 18FFDG PET/MR in comparison to PET/CT for evaluation of malignant bone lesions. J Nucl Med. 2014; 55(2):191–197. [PubMed: 24309383]
14. Beiderwellen K, Huebner M, Heusch P, et al. Whole-body [^{1}8F]FDG PET/MRI vs. PET/CT in the assessment of bone lesions in oncological patients: initial results. Eur Radiol. 2014; 24(8):2023–2030. [PubMed: 24907940]
15. Drzezga A, Souvatzoglou M, Eiber M, et al. First clinical experience with integrated whole-body PET/MR: comparison to PET/CT in patients with oncologic diagnoses. J Nucl Med. 2012; 53(6): 845–855. [PubMed: 22534830]
16. Jeong JH, Cho IH, Kong EJ, Chun KA. Evaluation of Dixon sequence on hybrid PET/MR compared with contrast-enhanced PET/CT for PET-positive lesions. Nucl Med Mol Imaging. 2014; 48(1):26–32. [PubMed: 24900135]
17. Heusch P, Nensa F, Schaarschmidt B, et al. Diagnostic accuracy of whole-body PET/MRI and whole-body PET/CT for TNM staging in oncology. Eur J Nucl Med Mol Imaging. 2015; 42(1):42–48. [PubMed: 25112399]
18. Huellner MW, Appenzeller P, Kuhn FP, et al. Whole-body nonenhanced PET/MR versus PET/CT in the staging and restaging of cancers: preliminary observations. Radiology. 2014; 273(3):859–869. [PubMed: 25102372]
19. Schäfer JF, Gatidis S, Schmidt H, et al. Simultaneous whole-body PET/MR imaging in comparison to PET/CT in pediatric oncology: initial results. Radiology. 2014; 273(1):220–231. [PubMed: 24877983]
20. Kuhn FP, Crook DW, Mader CE, Appenzeller P, von Schulthess GK, Schmid DT. Discrimination and anatomical mapping of PET-positive lesions: comparison of CT attenuation-corrected PET images with coregistered MR and CT images in the abdomen. Eur J Nucl Med Mol Imaging. 2013; 40(1):44–51. [PubMed: 22955547]
21. Pace L, Nicolai E, Luongo A, et al. Comparison of whole-body PET/CT and PET/MRI in breast cancer patients: lesion detection and quantitation of 18F-deoxyglucose uptake in lesions and in normal organ tissues. Eur J Radiol. 2014; 83(2):289–296. [PubMed: 24331845]
22. Taneja S, Jena A, Goel R, Sarin R, Kaul S. Simultaneous whole-body ^{1}8F-FDG PET-MRI in primary staging of breast cancer: a pilot study. Eur J Radiol. 2014; 83(12):2231–2239. [PubMed: 25282709]
23. Raad RA, Friedman KP, Heacock L, Ponzo F, Melsaether A, Chandarana H. Outcome of small lung nodules missed on hybrid PET/MRI in patients with primary malignancy. J Magn Reson Imaging. 2016; 43(2):504–511. [PubMed: 26192731]
24. Pujara AC, Raad RA, Ponzo F, et al. Standardized uptake values from PET/MRI in metastatic breast cancer: an organ-based comparison with PET/CT. Breast J. 2016 Feb.4 [Epub ahead of print].
25. Brix G, Nosske D, Lechel U. Radiation exposure of patients undergoing whole-body FDG-PET/CT examinations: an update pursuant to the new ICRP recommendations. Nuklearmedzi. 2014; 53(5): 217–220.

26. The 2007 Recommendations of the International Commission on Radiological Protection. ICRP publication 103. Ann ICRP. 2007; 37(2–4):1–332.
27. Huda W, Ogden KM, Khorasani MR. Converting dose-length product to effective dose at CT. Radiology. 2008; 248(3):995–1003. [PubMed: 18710988]
28. Huda W, Magill D, He W. CT effective dose per dose length product using ICRP 103 weighting factors. Med Phys. 2011; 38(3):1261–1265. [PubMed: 21520838]
29. Rauscher I, Eiber M, Fürst S, et al. PET/MR imaging in the detection and characterization of pulmonary lesions: technical and diagnostic evaluation in comparison to PET/CT. J Nucl Med. 2014; 55(5):724–729. [PubMed: 24652827]
30. Schwenzer NF, Schraml C, Müller M, et al. Pulmonary lesion assessment: comparison of whole-body hybrid MR/PET and PET/CT imaging—pilot study. Radiology. 2012; 264(2):551–558. [PubMed: 22653189]
31. Catalano OA, Nicolai E, Rosen BR, et al. Comparison of CE-FDG-PET/CT with CE-FDG-PET/MR in the evaluation of osseous metastases in breast cancer patients. Br J Cancer. 2015; 112(9):1452–1460. [PubMed: 25871331]
32. Moy L, Noz ME, Maguire GQ Jr, et al. Role of fusion of prone FDG-PET and magnetic resonance imaging of the breasts in the evaluation of breast cancer. Breast J. 2010; 16(4):369–376. [PubMed: 20443788]
33. Kumar R, Chauhan A, Zhuang H, Chandra P, Schnall M, Alavi A. Clinicopathologic factors associated with false negative FDG-PET in primary breast cancer. Breast Cancer Res Treat. 2006; 98(3):267–274. [PubMed: 16555126]
34. Anders CK, Johnson R, Litton J, Phillips M, Bleyer A. Breast cancer before age 40 years. Semin Oncol. 2009; 36(3):237–249. [PubMed: 19460581]
35. Surveillance, Epidemiology and End Results (SEER) Program. Cancer Statistics Review (1975–2012). National Cancer Institute, DCCPS, Surveillance Research Program, Surveillance Research Branch, released April 2015 based on the November 2014 submission. [Accessed August 7, 2015] http://seer.cancer.gov/csr/1975_2012/browse_csr.php?sectionSEL=4&pageSEL=sect_04_table.13.html.
36. van Straten M, Deak P, Shrimpton PC, Kalender WA. The effect of angular and longitudinal tube current modulations on the estimation of organ and effective doses in x-ray computed tomography. Med Phys. 2009; 36(11):4881–4889. [PubMed: 19994496]
37. Hicks DG, Short SM, Prescott NL, et al. Breast cancers with brain metastases are more likely to be estrogen receptor negative, express the basal cytokeratin CK5/6, and overexpress HER2 or EGFR. Am J Surg Pathol. 2006; 30(9):1097–1104. [PubMed: 16931954]

Advances in Knowledge

- Diffusion-weighted and contrast-enhanced PET/MR imaging sequences depicted distant (100% for readers 1 and 2) and axillary (100% for reader 1, 88% for reader 2) metastatic disease at rates similar to those of PET/CT (96% for readers 3 and 4, $P = .50$; 88% for readers 3 and reader 4, $P > .99$).
- Diffusion-weighted and contrast-enhanced PET/MR imaging sequences yielded higher lesion-level sensitivity for liver (100% for reader 1, 80% for reader 2 vs 75% for reader 3, 70% for reader 4; $P < .001$) and possibly bone (98% for reader 1, 95% for reader 2 vs 99% for reader 3, 87% for reader 4; $P = .012$) metastases as compared with unenhanced PET/CT.
- In the setting of a supine whole-body examination, diffusion-weighted and contrast-enhanced PET/MR imaging sequences are more sensitive per patient for breast cancers (17 of 17 [100%] for readers 1 and 2 vs 11 of 17 [65%] for reader 3 and 10 of 17 [59%] for reader 4) than is PET/CT ($P < .001$).

Implications for Clinical Care

- In patients with breast cancer who are undergoing metastatic work-up, FDG PET/MR imaging can be substituted for PET/CT, with the caveat that PET/MR imaging may yield decreased sensitivity for lung metastases.
- PET/MR imaging with diffusion-weighted and contrast-enhanced imaging should be considered, especially when the detection of liver or brain metastases, respectively, could lead to treatment change.
- PET/MR imaging is encouraged when radiation dose is of particular concern, for example in young patients and in patients undergoing serial PET-based examinations.

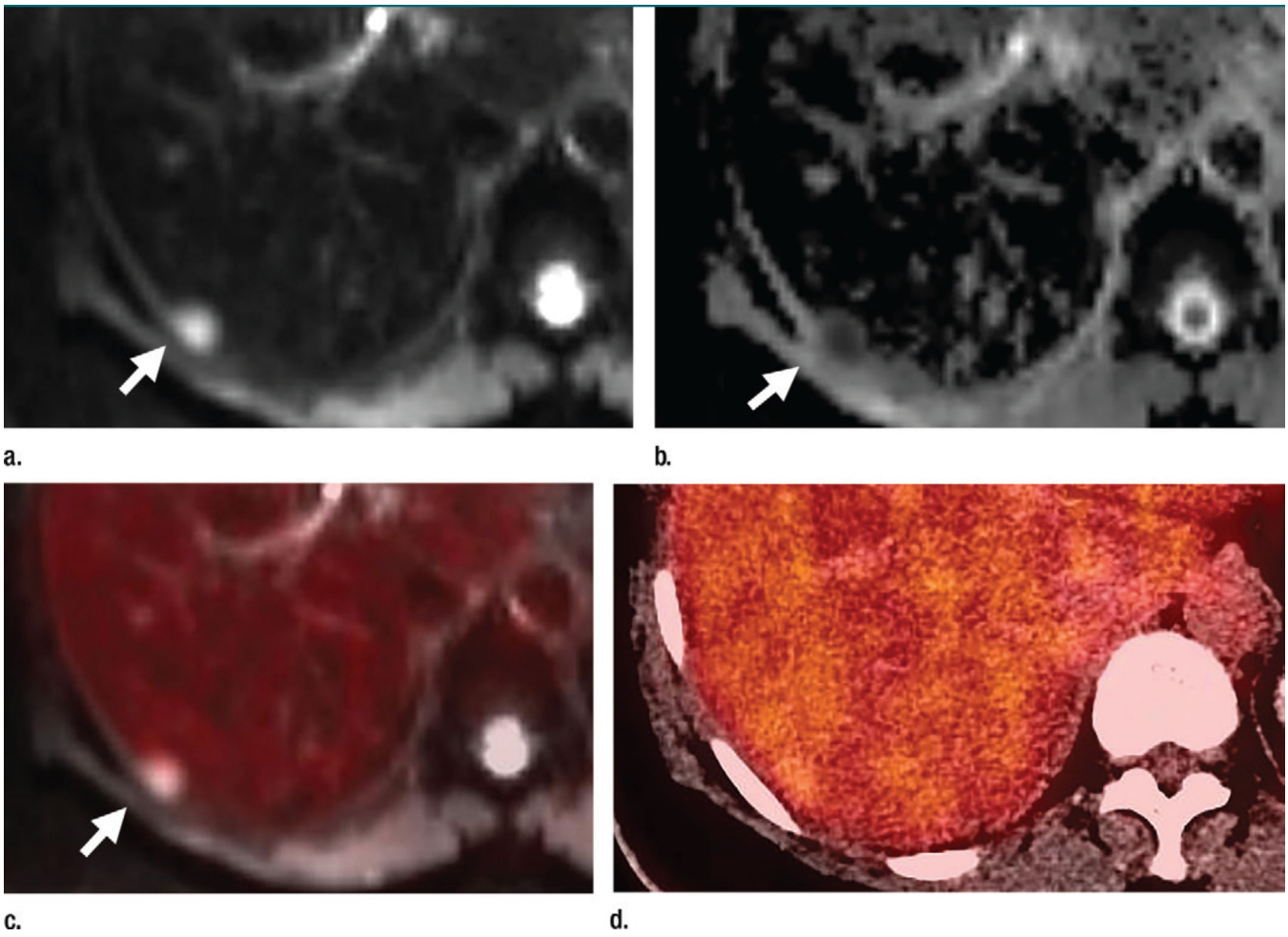

Figure 1.

Axial **(a–c)** PET/MR and **(d)** PET/CT images in a 64-year-old woman with a history of left breast cancer metastatic to lung and bone obtained to monitor response during chemotherapy. A liver metastasis (arrow) is seen on the PET/MR images (**a–c**) but not on the PET/CT image (**d**). The metastasis is best seen as an area of high signal intensity on the diffusion-weighted image (**a**), with corresponding low signal intensity on the apparent diffusion coefficient map (**b**). There is minimal corresponding FDG uptake on the fused diffusion-weighted and PET image (**c**). This metastasis was also seen on contrast-enhanced T1-weighted images (not shown). This metastasis is not seen on PET/CT images (**d**).

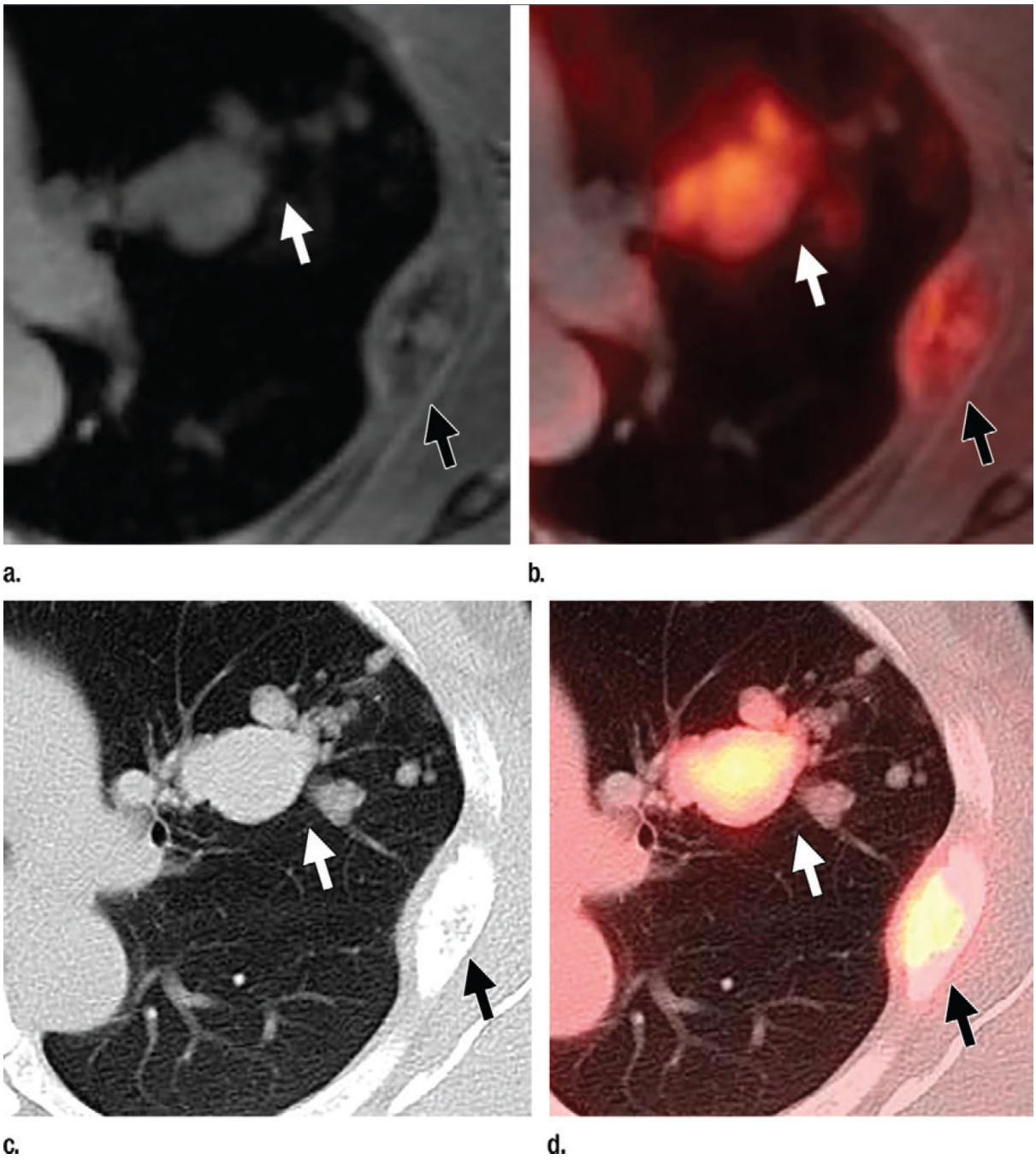

Figure 2.

Axial images in a 48-year-old woman with a history of left breast cancer metastatic to lung and bone obtained to monitor response during chemotherapy. **(a)** Contrast-enhanced T1-weighted MR and **(b)** T1-weighted MR/PET images show several lung metastases (white arrow). **(c)** B60 kernel CT and **(d)** PET/CT images show these metastases (white arrow) more clearly. An expansile rib metastasis (black arrow) is seen on all images.

Table 1

Sensitivity and Specificity for the Presence of at Least One Systemic Metastasis, Breast Cancer, and Axillary Nodal Metastasis for Each Reader

Modality, Reader, and Statistic	Systemic Metastasis*		Breast Cancers		Axillary Nodal Metastasis	
	Sensitivity	Specificity	Sensitivity	Specificity	Sensitivity	Specificity
PET/MR imaging						
Reader 1	100 (30/30)	86 (18/21)	100 (17/17)	97 (33/34)	100 (8/8)	95 (41/43)
Reader 2	100 (30/30)	90 (19/21)	100 (17/17)	97 (33/34)	88 (7/8)	95 (41/43)
95% CI	92, 100	76, 95	90, 100	90, 100	69, 97	88, 98
PET/CT						
Reader 3	97 (28/29*)	77 (17/22)	59 (10/17)	100 (34/34)	88 (7/8)	95 (41/43)
Reader 4	97 (28/29*)	82 (18/22*)	65 (11/17)	100 (34/34)	88 (7/8)	95 (41/43)
95% CI	88, 99	64, 91	42, 79	94, 100	64, 99	88, 98
P value	.500	.219	<.001	.500	>.99	>.99

Note.—Unless otherwise indicated, data are percentages. Data in parentheses are raw data. CI = confidence interval.

*One patient had a brain metastasis that was seen on only PET/MR images. He was not counted as having metastatic disease because the same-day PET/CT examination did not extend to the vertex.

Table 2

Systemic Metastatic Lesion Detection

	PET/MR Imaging		PET/CT		
Metastasis Location	**Reader 1**	**Reader 2**	**Reader 3**	**Reader 4**	***P* Value**
Liver (*n* = 40)					<.001
No. of true-positive findings	40	32	30	28	…
No. of false-positive findings	1	0	1	0	…
Sensitivity	100 (92, 100)	80 (66, 91)	75 (58, 87)	70 (54, 83)	…
Lung (*n* = 23)					.065
No. of true-positive findings	20	17	23	22	…
No. of false-positive findings	8	7	12	10	…
Sensitivity	87 (68, 96)	74 (53, 88)	100 (87, 100)	96 (79, 99)	…
Pleura (*n* = 16)					>.99
No. of true-positive findings	16	16	16	16	…
No. of false-positive findings	0	0	0	0	…
Sensitivity	100 (80, 100)	100 (80, 100)	100 (80, 100)	100 (80, 100)	…
Distant lymph node (*n* = 41)					.083
No. of true-positive findings	39	38	39	35	…
No. of false-positive findings	3	3	3	4	…
Sensitivity	95 (83, 99)	92 (80, 98)	95 (83, 99)	85 (72, 93)	…
Bone (*n* = 107)					.012
No. of true-positive findings	105	102	106	90	…

	PET/MR Imaging		PET/CT		
Metastasis Location	**Reader 1**	**Reader 2**	**Reader 3**	**Reader 4**	***P* Value**
No. of false-positive findings	1	0	5	0	…
Sensitivity	98 (94, 100)	95 (90, 98)	99 (95, 100)	87 (79, 92)	
Brain*					NA
No. of true-positive findings	15	14	0	0	…
No. of false-positive findings	0	0	1 imaged	1 imaged	…
Sensitivity	100 (79, 100)	93 (70, 100)	NA	NA	…

Note.—Data in parentheses are 95% confidence intervals. NA = not applicable.

*Because of issues with our protocol, the brain was included in 24 of the 51 PET/CT examinations and in only one of five patients found to have brain metastases at PET/MR imaging.

Radiology. Author manuscript; available in PMC 2016 October 01.

Table 3

Sensitivity and Specificity of Each Modality by Using Data from Both Readers Who Provided Data for That Modality

	Sensitivity		Specificity	
Metastasis Location	**PET/MR**	**PET/CT**	**PET/MR**	**PET/CT**
Liver	78.3, 99.8	50.0, 88.4	92.2, 99.9	94.5, 100
Lung	61.5, 99.8	73.5, 100	80.8, 96.3	70.5, 89.6
Pleura	73.5, 100	73.5, 100	94.9, 100	94.9, 100
Distant lymph node	78.3, 99.8	66.4, 95.2	90.3, 99.7	88.0, 99.7
Bone	90.9, 100	84.4, 99.7	92.8, 100	90.4, 99.9

Note.—Data are 95% confidence intervals.

Table 4

Number of True-Positive and False-Positive Lesions Detected by Each Reader with Each Imaging Sequence

Metastasis or Cancer Location	Reader 1	Reader 2	Reader 3	Reader 4
Breast (n = 18)				
Total *	18, 1	18, 1	11, 0	12, 0
True-positive findings †	14, 16, 18	14, 16, 18	11, 11	12, 12
False-positive findings ‡	1, 1, 1	1, 1, 1	0, 0	0, 0
Axillary nodes (n = 19)				
Total *	19, 3	18, 2	17, 5	17, 3
True-positive findings †	19, 19, 18	18, 18, 17	17, 17	17, 17
False-positive findings ‡	3, 3, 3	2, 2, 2	5, 3	3, 3
Liver (n = 40)				
Total *	40, 1	32, 0	30, 1	28, 0
True-positive findings †	28, 40, 27	25, 32, 26	27, 23	25, 22
False-positive findings ‡	0, 1, 0	0, 0, 0	1, 0	0, 0
Lung (n = 23)				
Total *	20, 8	17, 7	23, 12	22, 10
True-positive findings †	20, 11, 18	17, 11, 16	19, 23	20, 22
False-positive findings ‡	6, 2, 7	5, 2, 4	3, 12	4, 10
Pleura (n = 16)				
Total *	16, 0	16, 0	16, 0	16, 0
True-positive findings †	16, 12, 16	16, 12, 16	16, 16	16, 16
False-positive findings ‡	0, 0, 0	0, 0, 0	0, 0	0, 0
Distant nodes (n = 41)				
Total *	39, 3	38, 3	35, 4	39, 3
True-positive findings †	39, 37, 34	38, 36, 30	35, 35	39, 32
False-positive findings ‡	3, 2, 2	3, 2, 2	4, 4	3, 3
Bone (n = 107)				
Total *	105, 1	102, 0	106, 5	93, 0
True-positive findings †	102, 105, 101	98, 102, 100	103, 82	92, 90
False-positive findings ‡	1, 1, 0	0, 0, 0	5, 2	0, 0
Brain (n = 15)				
Total *	15, 0	14, 0	NA	NA
True-positive findings †	0, 7, 15	0, 7, 14	NA	NA

Note.—NA = not applicable.

* Data are number of true-positive findings and number of false-positive findings, respectively.

[†]Data are number of true-positive PET, diffusion-weighted, and contrast-enhanced T1-weighted MR imaging findings, respectively.

[‡]Data are number of false-positive PET, diffusion-weighted, and contrast-enhanced T1-weighted MR imaging findings, respectively.